Wireless Pers Commun (2013) 71:243–254
DOI 10.1007/s11277-012-0813-1

Study of Magnetic Field Coupling Technologies in Activating RFID-SIM Card Mobile Payments

Yejun He

Published online: 29 September 2012

Abstract In this paper, we propose a RFID (Radio-frequency Identification)-SIM card mobile payment scheme and study the magnetic field coupling technologies in activating the payments for the second generation readers. Simulation results show that the mobile payment scheme based on a low-frequency magnetic-coupling activation strategy is reasonable, secured, robust, low-cost, and easy to promote. The performance of various mobile phones integrated with the RFID-SIM cards is very similar under the proposed activation strategy. The activation distances between various mobiles and the readers are very consistent. When high-frequency magnetic coupling is used, however, the performance of different mobile phones shows great difference because of the small attenuation factor.

Keywords Magnetic field coupling · RFID · Mobile payment · NFC

1 Introduction

Mobile payment is an important part of building a "smart earth". It is also a kind of service that allows users to pay for the goods or service through mobile phones. At home and abroad, there are three types of mobile payment solutions: a 13.56 MHz contactless NFC (near field communication) proximity communications solution (used in Japan, Korea, France, etc.) [1], a 13.56 MHz affixed card solution (a 13.56 MHz card is attached to the rear cover of a mobile phone), and a 2.4 GHz RFID-SIM card solution (developed by the Nationz Technologies Inc., China). The 13.56 MHz contactless NFC proximity communications solution is usually realized by a 13.56 MHz RFID identification system. Specifically, the RFID smart label is affixed to the cover of the battery of a mobile phone in order to save space optimally [2].

This work was supported by the National Natural Science Foundations of China (No. 60972037), the Fundamental Research Program of Shenzhen City (No. JC200903120101A, No. JC201005250067A) and the International Cooperative Program of Shenzhen City (ZYA201106090040A).

Y. He (✉)
College of Information Engineering, Shenzhen University, Shenzhen 518060, China
e-mail: heyejun@126.com; heyejun@ieee.org

The use of such kind of RFID mobile phones is pervasively adopted Japan and South Korea. However, its application is very limited since the 13.56 MHz affixed card solution cannot be integrated with the mobile SIM. Compared with Korea and Japan, China starts relatively late in terms of research and applications of high-frequency RFID. However, with the build up of relevant infrastructure equipment and a better understanding of the advantages of RFID systems, China has made rapid progress in developing and applying RFID technologies in recent years.

The conventional mobile-payment activation strategy (sometimes called "distance control scheme") operates in the 2.4 GHz frequency band and with an increasingly widespread applications of RFID. In this setting, the interference problem is critical: the identification distance is much shorter than the designed operating distance; and the readers and the tags do not communicate resulting in failures of the reading procedures. In this paper, we propose a RFID-SIM card mobile payment scheme in which the activating strategy for the second generation readers is based on magnetic field coupling with a low frequency signal [3]. The rest of this paper is organized as follows. In Sect. 2, we describe our proposed RFID-SIM card mobile payment scheme. In Sect. 3, we give a detailed theoretical study of the activation strategy with magnetic field coupling. Simulation results and discussions are presented in Sect. 4 and a conclusion is given in Sect. 5.

2 Proposed RFID-SIM Card Mobile Payment Scheme

2.1 Block Diagram

The proposed RFID-SIM card mobile payment scheme is shown in Fig. 1. Here, RSSI denotes received signal strength indicator, which is a measurement of the power of a received radio signal. Tx and Rx stand for transmit and receive, respectively and LF means low frequency.

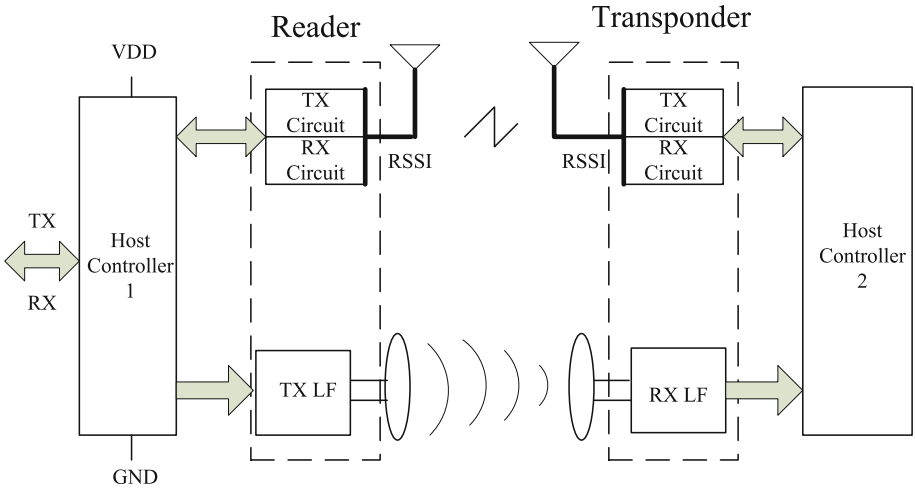

Fig. 1 Block diagram of 2.4G RFID-SIM card system with a low-frequency magnetic-coupling activation strategy

2.2 Working Principles

The conventional RFID-SIM card mobile payment schemes adopt an activation strategy (or "distance control scheme") operating in the 2.4 GHz frequency band. The RSSI is the main parameter for consideration. Due to some drawbacks, we propose a new generation activation strategy. Moreover, the new generation RFID-SIM card system provides good compatibility with previous communication protocols.

In the proposed 2.4G RFID-SIM card system, the 2.4 GHz transceiver only perform two-way data communications while the LF transmitter generates a low frequency signal. The basic operating principle is as follows. The reader continuously sends random data and respective information group frame via the LF transmitter. The contactless card is activated and return the received data to the reader through the 2.4 GHz radio frequency. The reader then decides if the communication object of the contactless card is the same reader through checking the data. In the meantime, the contactless card also compares the received magnetic field data with the received 2.4 GHz RF data to confirm that the same reader generates the two data. This scheme avoids wrong operations when the operating distance is out of the designed range. The new generation contactless card is also easily activated by magnetic field (similar to the old contactless card with frequently wakeup in energy saving). The new generation contactless card places received low-frequency magnetic field data to the default word segment of original ATI (answer to inquiry) message to guarantee the compatibility with old reader. To support an old card, the new generation reader decides if the value of the default word segment is saved according to the card type information included in ATI message.

2.3 Reader

The reader includes two CPUs as shown in Fig. 2: one is the master CPU and the other is the slave CPU. The reader also contains a triangular wave generator, an amplifier and a driver. The two CPUs possess the following functions. The master CPU is responsible for the 2.4 GHz protocol process, low frequency IDr (identity of random) data generation,and the serial port protocol process in POS. The slave CPU performs data coding and transmission, i.e., receives the IDr data from the master CPU, compose the IDr data frame with scrambling and Manchester code coding. Figure 2 shows that the master CPU uses soft serial port while the slave CPU uses hard serial port.

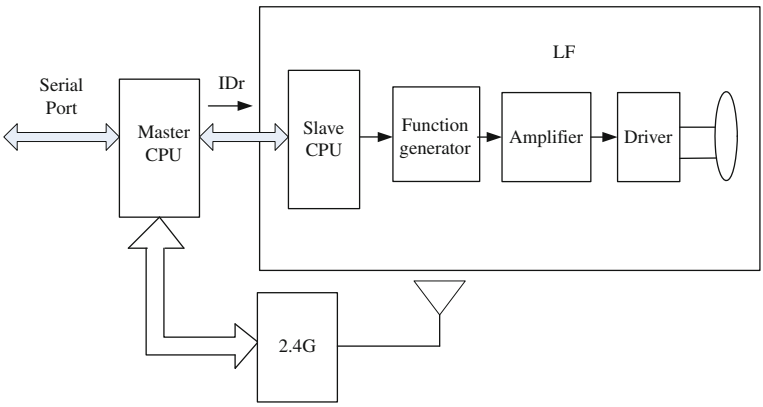

Fig. 2 Block diagram of reader

3 The Activation Strategy with Magnetic Field Coupling

3.1 Activation Strategy

The block diagram of the new generation of activation strategy with magnetic coupling is shown in Fig. 3. The activation decision is based on the coupling voltage in the SIM-card coil. Magnetic field coupling occurs between the reader coil and the transponder (SIM-card coil). The reader produces time-changing magnetic field and the inductance coil in the transponder will produce an induced voltage. When the transponder is close enough such that the induced voltage in the transponder reaches a threshold value, information verification begins and the "swipe card" procedure is initiated.

The inductive voltage in the transponder is directly proportional to the rate of change of the total magnetic flux ψ through the surface surrounded by the SIM card coil. The induced voltage V_2 is given by

$$V_2 = -\frac{d\psi}{dt} = -N_2\frac{d\phi}{dt} \tag{1}$$

where N_2 denotes the number of turns in the coil of the transponder and ϕ stands for the magnetic flux through each turn. The SIM card in the transponder can determine the distance to the reader based on the voltage amplitude of V_2∘

3.2 The Magnetic Flux Density Near the Reader Coil with Rectangular

If the reader coil is rectangular in shape, the components of the magnetic flux density in space are given by

$$B_x = \frac{\mu_0 I z}{4\pi\left[(l_1-x)^2+z^2\right]}\left(\frac{l_2+y}{\sqrt{(l_1-x)^2+(l_2+y)^2+z^2}}+\frac{l_2-y}{\sqrt{(l_1-x)^2+(l_2-y)^2+z^2}}\right) - \frac{\mu_0 I z}{4\pi\left[(l_1+x)^2+z^2\right]}\left(\frac{l_2-y}{\sqrt{(l_1+x)^2+(l_2-y)^2+z^2}}+\frac{l_2+y}{\sqrt{(l_1+x)^2+(l_2+y)^2+z^2}}\right) \tag{2}$$

$$B_y = \frac{\mu_0 I z}{4\pi\left[(l_2-y)^2+z^2\right]}\left(\frac{l_1-x}{\sqrt{(l_1-x)^2+(l_2-y)^2+z^2}}+\frac{l_1+x}{\sqrt{(l_1+x)^2+(l_2-y)^2+z^2}}\right)$$

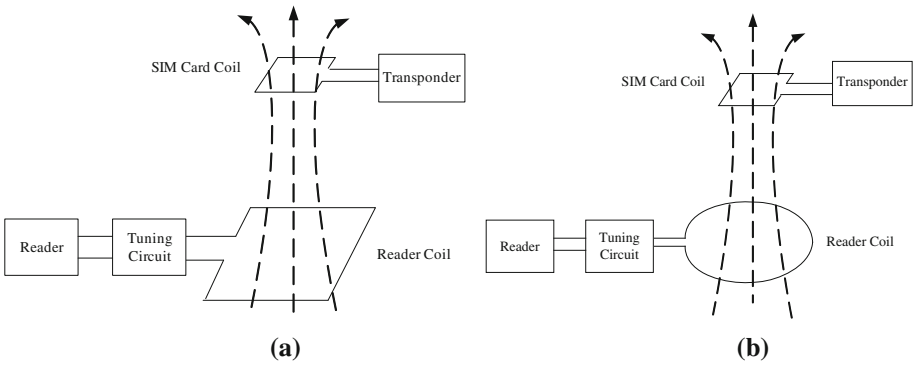

Fig. 3 New generation of activation strategy with magnetic coupling

$$-\frac{\mu_0 I z}{4\pi\left[(l_1+y)^2+z^2\right]}\left(\frac{l_1+x}{\sqrt{(l_1+x)^2+(l_2+y)^2+z^2}}+\frac{l_1-x}{\sqrt{(l_1-x)^2+(l_2+y)^2+z^2}}\right) \tag{3}$$

$$\begin{aligned}B_z=&\frac{\mu_0 I(l_2+y)}{4\pi\left[(l_2+y)^2+z^2\right]}\left(\frac{l_1+x}{\sqrt{(l_1+x)^2+(l_2+y)^2+z^2}}+\frac{l_1-x}{\sqrt{(l_1-x)^2+(l_2+y)^2+z^2}}\right)\\&+\frac{\mu_0 I(l_2-y)}{4\pi\left[(l_2-y)^2+z^2\right]}\left(\frac{l_1-x}{\sqrt{(l_1-x)^2+(l_2-y)^2+z^2}}+\frac{l_1+x}{\sqrt{(l_1+x)^2+(l_2-y)^2+z^2}}\right)\\&+\frac{\mu_0 I(l_1-x)}{4\pi\left[(l_1-x)^2+z^2\right]}\left(\frac{l_2+y}{\sqrt{(l_1-x)^2+(l_2+y)^2+z^2}}+\frac{l_2-y}{\sqrt{(l_1-x)^2+(l_2-y)^2+z^2}}\right)\\&+\frac{\mu_0 I(l_1+x)}{4\pi\left[(l_1+x)^2+z^2\right]}\left(\frac{l_2-y}{\sqrt{(l_1+x)^2+(l_2-y)^2+z^2}}+\frac{l_2+y}{\sqrt{(l_1+x)^2+(l_2+y)^2+z^2}}\right)\end{aligned} \tag{4}$$

Substituting (2) to (4) into $B=\sqrt{B_x^2+B_y^2+B_z^2}$ leads to the magnetic flux density of any point in space. When $x=0$ and $y=0$, the magnetic flux density in the vertical direction z (perpendicular to the rectangular coil plane) is given by

$$B=\frac{N_1\mu_0 I l_1 l_2}{\pi}\left(\frac{1}{(l_2^2+z^2)\sqrt{l_1^2+l_2^2+z^2}}+\frac{1}{(l_1^2+z^2)\sqrt{l_1^2+l_2^2+z^2}}\right) \tag{5}$$

where l_1 and l_2 are, respectively, equal to half the length and width of the rectangular coil; N_1 denotes the number of turns of the reader coil; I denotes the reader coil current; and μ_0 denotes the permeability of air or vacuum.

3.3 The Magnetic Flux Density Near the Reader Coil with Circular

If the reader coil is circular in shape, the components of the magnetic flux density in space are given by

$$B_x=\frac{\mu_0 I r}{2N_{\max}}\sum_{n=1}^{N_{\max}}\frac{z\cos((n-\frac{1}{2})\frac{2\pi}{N_{\max}})}{\left[(x-r\cos((n-\frac{1}{2})\frac{2\pi}{N_{\max}}))^2+(y-r\sin((n-\frac{1}{2})\frac{2\pi}{N_{\max}}))^2+z^2\right]^{\frac{3}{2}}} \tag{6}$$

$$B_y=\frac{\mu_0 I r}{2N_{\max}}\sum_{n=1}^{N_{\max}}\frac{z\sin((n-\frac{1}{2})\frac{2\pi}{N_{\max}})}{\left[(x-r\cos((n-\frac{1}{2})\frac{2\pi}{N_{\max}}))^2+(y-r\sin((n-\frac{1}{2})\frac{2\pi}{N_{\max}}))^2+z^2\right]^{\frac{3}{2}}} \tag{7}$$

$$B_z=\frac{\mu_0 I r}{2N_{\max}}\sum_{n=1}^{N_{\max}}\frac{r-y\sin((n-\frac{1}{2})\frac{2\pi}{N_{\max}})-x\cos((n-\frac{1}{2})\frac{2\pi}{N_{\max}})}{\left[(x-r\cos((n-\frac{1}{2})\frac{2\pi}{N_{\max}}))^2+(y-r\sin((n-\frac{1}{2})\frac{2\pi}{N_{\max}}))^2+z^2\right]^{\frac{3}{2}}} \tag{8}$$

where I denotes the reader coil current; r is the radium of the circular coil; μ_0 denotes the permeability of air or vacuum; $N_{\max}$ denotes the number of segment in the numerical integral ($N_{\max}=1,000$). Substituting (6) to (8) into $B=\sqrt{B_x^2+B_y^2+B_z^2}$ leads to the magnetic

flux density of any point in space. When $x = 0$ and $y = 0$, the magnetic flux density in the vertical direction z (perpendicular to the circular coil plane) is given by

$$B = \mu_0 H = \frac{\mu_0 I N_1 a^2}{2(a^2 + z^2)^{3/2}} \tag{9}$$

3.4 Coupling Voltage Based on Magnetic Flux Density

According to the changing magnetic-flux principle, if the signal in the reader coil is a sine wave, the amplitude of the induced voltage for the SIM-card coil (the coupling coil) will be given by [4]

$$V_0 = 2\pi f N_2 Q S B \cos\alpha \tag{10}$$

where N_2 denotes the number of turns of the coupling coil; Q is the quality factor of the resonant circuit; S is the area of the coupling coil; B is the magnetic flux density through the coupling coil in square meters; α is the angle of arrival of the signal or angle between the reader coil and the coupling coil. In Fig. 3, the reader coil plane is parallel to the coupling coil plane and thus $\alpha = 0$. On the other hand, if the signal in the reader coil is a triangular wave, the amplitude of the induced voltage for the SIM-card coil (the coupling coil) will be given by [4]

$$V_0' = 4 f N_2 Q S B \cos\alpha \tag{11}$$

If the shielding material is considered, i.e, the magnetic field attenuation factor takes the form $A = e^{(-t\sqrt{\pi f \mu \gamma})}$ (t, μ and γ denote the thickness, the permeability and conductivity of the shielding material, respectively), then Eqs. (10) and (11) need to be multiplied by A.

4 Simulation Results

Due to the limited space, we only consider the case of a triangular wave and a circular reader coil. The simulation parameters are as follows: diameter of the reader coil is 180 mm, number of turns is 110, diameter of the copper conductor is 0.6 mm. The coupling coil uses a rectangular coil with a length of 24 mm, a width of 14 mm and 4 turns. The frequencies used are 2 kHz, 10 kHz and 2 MHz.

According to the model shown in Fig. 3, we simulate the coupling voltage of the coupling coil corresponding to different input signal (excitation source) of the reader coil, including time-changing current and time-changing voltage.

4.1 Excitation Source with Time-Changing Current

We take an excitation source with a triangular time-changing current. The amplitude of the triangular wave in the reader coil is 1.83A. Using Matlab simulation, we obtain the space distributions of the induced voltage (coupling voltage) at 2 kHz and 3 MHz and plot them in Figs. 4 and 5, respectively. Figure 4a, b show the induced voltage when the reader coil is at a height of 10 and 500 mm, respectively. Similar results can be found in Fig. 5. Comparing Fig. 4 with Fig. 5, we can see that the higher the frequency is, the bigger the coupling voltage is.

Figure 6 shows that the induced voltage along the z-axis is directly proportional to the operating frequency. The smaller the z value is, i.e. the coupling coil is closer to the reader coil, the bigger the induced voltage is. The reason is $V_o = -M(di/dt)$.

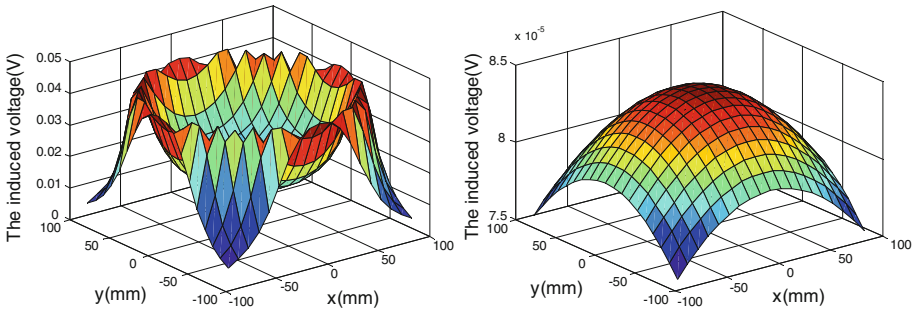

(a) height z=10mm **(b)** height z=500mm

Fig. 4 The space distribution of the induced voltage at different heights (Operating frequency = 2 kHz)

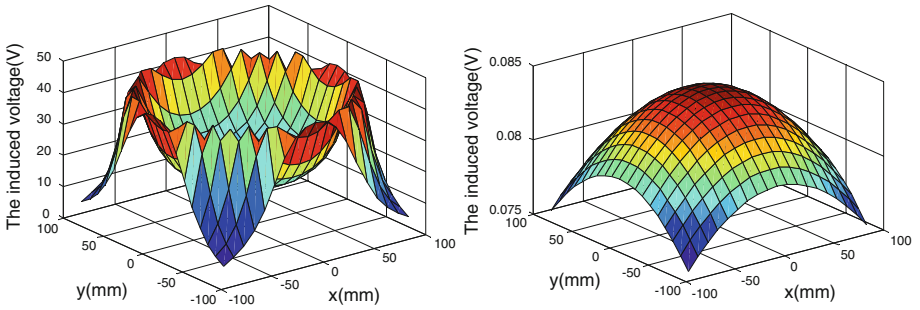

(a) height z= 10mm **(b)** height z=500mm

Fig. 5 The space distribution of the induced voltage at different heights (Operating frequency = 2 MHz)

Fig. 6 The coupling voltage vs. frequency for current excitation

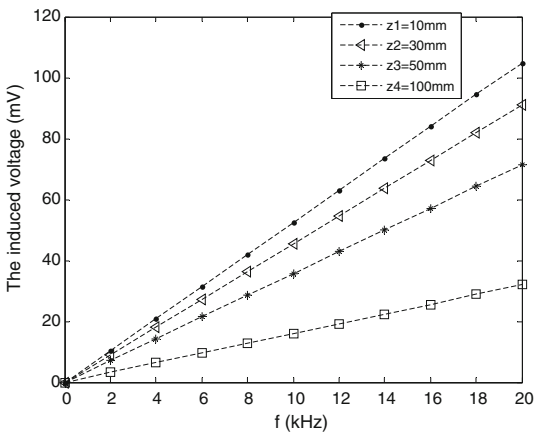

However, it is very difficult to produce time-varying current sources in practical applications, we suggest and discuss using an excitation source with a time-changing voltage in the next section.

4.2 Excitation Source with Time-Changing Voltage

The voltage amplitude of the triangular wave in the reader coil is 15V. When the frequencies are set at 2 kHz,5 kHz, and 2 MHz, respectively, the space distribution of the induced voltage (coupling voltage) are shown in Figs. 7, 8, and 9, respectively. Results show that the induced voltage is the largest at a frequency of 5kHz compared with those induced at 2 kHz and 2 MHz.

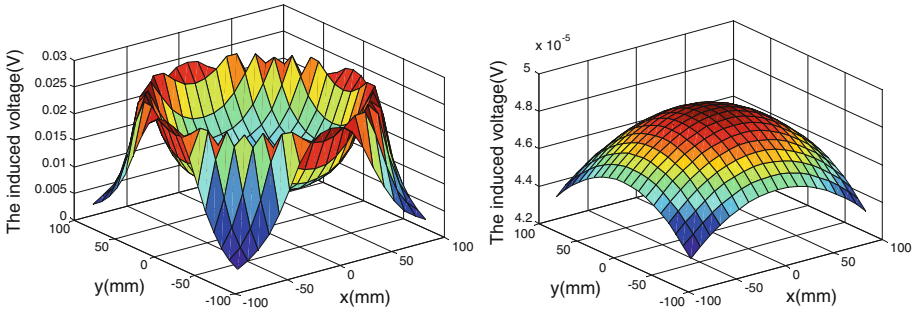

(a) height z=10mm **(b)** height z=500mm

Fig. 7 The space distribution of the induced voltage at different heights (Operating frequency = 2 kHz)

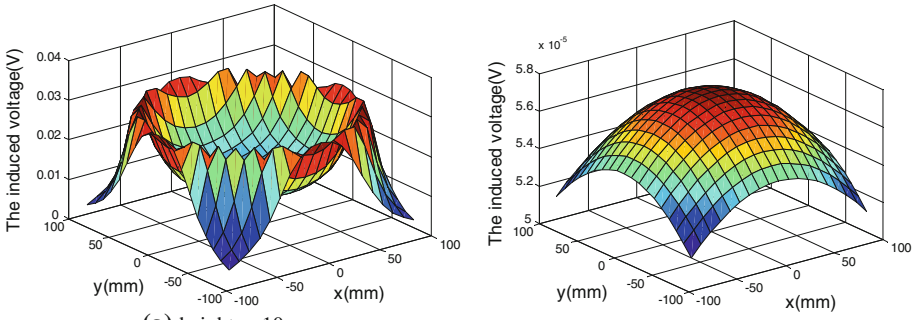

(a) height z=10mm **(b)** height z=500mm

Fig. 8 The space distribution of the induced voltage at different heights (Operating frequency = 5 kHz)

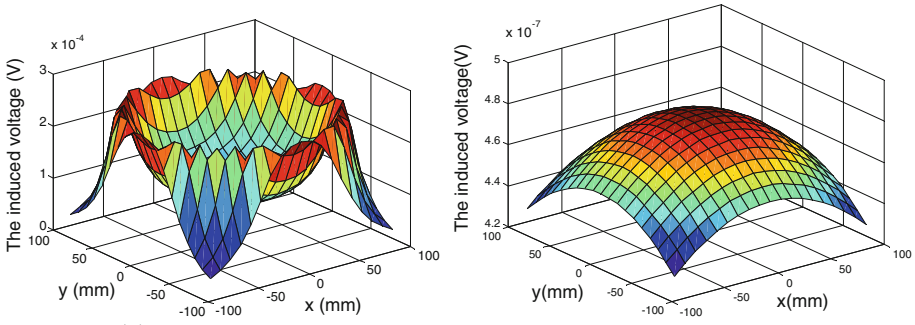

(a) height z= 10mm **(b)** height z=500 mm

Fig. 9 The space distribution of the induced voltage at different heights (Operating frequency = 2 MHz)

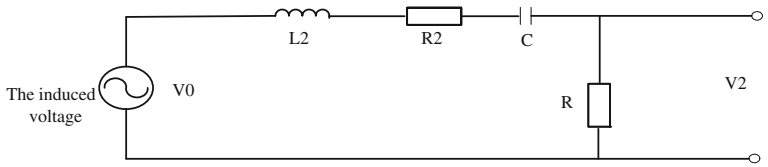

Fig. 10 The equivalent circuit

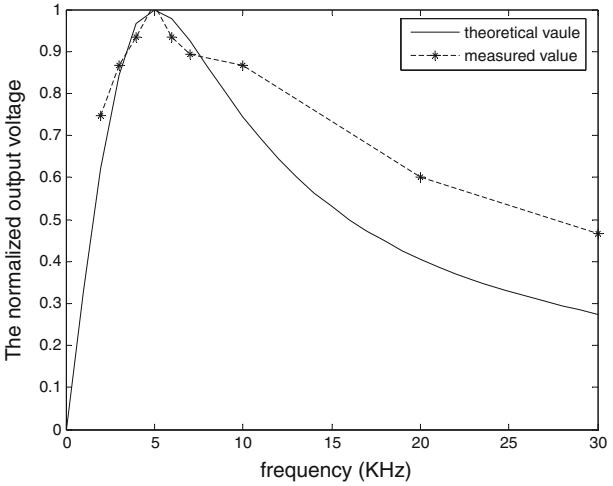

Fig. 11 The normalized output voltage vs. frequency

In a practical system, we need to consider the equivalent circuit shown in Fig. 10. Here, L_2 denotes the inductance of the coupling coil, we will take an inductance equation found in [5]; R_2 is the resistance of the coupling coil $R_2 = 0.04\Omega$); R and C are followed by the amplifier ($R = 1\Omega$, $C = 650uF$). In the theoretical simulation, we set Q as 5. If R is much larger than $R_2(R = 1\Omega, R_2 = 0.04\Omega)$, then

$$Q = \frac{\omega_0 L}{R_2 + R} \approx \frac{\omega_0 L}{R} = \frac{1}{R\omega_0 C} \tag{12}$$

$$\omega_0 = \frac{1}{\sqrt{L_2 C}} \tag{13}$$

The resonant frequency is calculated as 5 kHz.

Refer to Fig. 11 (z = 500 mm), the peak value of the coupling voltage along the z-axis is given by

$$V_0 = 4fN_2QS\frac{\mu_0 l_1 l_2 N_1}{\pi}\left(\frac{1}{(l_2^2+z^2)\sqrt{l_1^2+l_2^2+z^2}} + \frac{1}{(l_1^2+z^2)\sqrt{l_1^2+l_2^2+z^2}}\right) \times \frac{V_1}{\sqrt{R_1^2+(\omega L_1)^2}} \tag{14}$$

where V_1 denotes the amplitude of the voltage of reader coil, R_1 and L_1 denote the resistance and the inductance of the reader coil, respectively. L_1 can be calculated in terms of equation found in [5]. Figure 11 shows the comparison between the theoretical value and the measured value for the output voltage $V_2(V_2$ is normalized). V_2 is given by

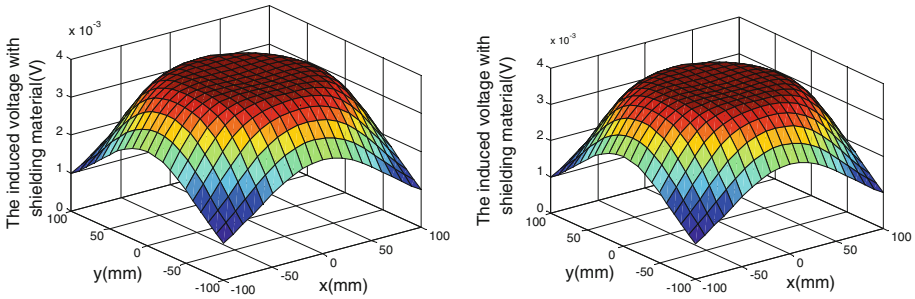

(a) with a shielding material **(b)** without a shielding material

Fig. 12 2 kHz(attenuation factor is 0.6)

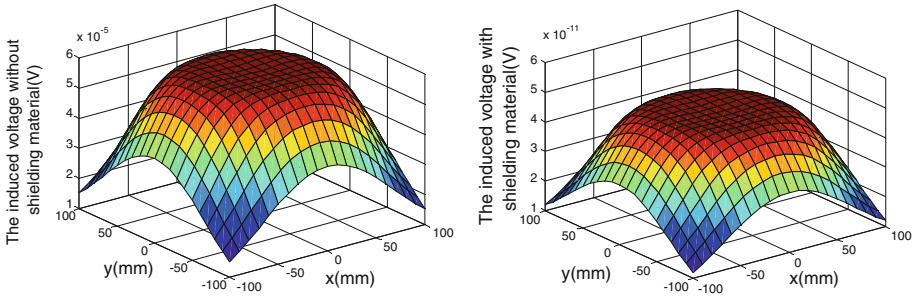

(a) with a shielding material **(b)** without a shielding material

Fig. 13 2 MHz(attenuation factor is 8×10^{-7})

$$V_2 = \frac{R}{\sqrt{(R+R_2)^2 + \left(\omega L_2 - \frac{1}{\omega C}\right)^2}} V_0 \tag{15}$$

The measured values in Fig. 11 is similar to the theoretical values.

4.3 The Induced Voltage with and Without Shielding Material

We consider the attenuation of the magnetic induction when a shielding material exists. Here, the shielding material mainly comes from the cell. The height z is 50 mm, the relative permeability of battery is 1. The conductivity is 10^6 S/m.

Figures 12 and 13 show that the low-frequency activation strategy does not result in obvious difference of the coupling voltage with and without the shielding material. On the contrary, the coupling voltage of the high-frequency activation scheme changes significantly with and without a shielding material. Therefore, we suggest adopting a low-frequency activation strategy in future RFID-SIM card systems.

5 Conclusion

In this paper, we have proposed a RFID-SIM card mobile payment scheme with a low-frequency magnetic coupling activation strategy. The excitation source uses a triangular wave. For a current excitation source, the induced voltage of the coupling coil is directly

proportional to frequency. For a voltage excitation source, the difference of the coupling voltage between the theoretical value and the measured value is resulted from the related parameters after the amplifier is connected to the coupling coil. When using an AC voltage feed, theoretical calculations and field tests have shown the following consistent results. At first, the coupling voltage increases with the increase of feed frequency. When resonance occurs, the coupling voltage is the maximum. Afterwards, the coupling voltage decreases with the increase of feed frequency. From the simulation of the coupling voltage of any point in space, we know that when the coupling coil is near the transmitting coil, the coupling voltage is relatively larger; when the height between the two coils increases, the coupling voltage is larger when the coupling coil is directly over the transmitting coil.

Acknowledgments The author would like to thank Jie Yang, Wei Zhang, Xiaorong Tang and Jiefeng Ao for many helpful discussions. He would also like to thank the Editor and the anonymous reviewers for their insights that improved the paper significantly.

References

1. Lacmanovic, I., Radulovic, B., & Lacmanovic, D. (2010). Contactless payment systems based on RFID technology, MIPRO 2010, May 24–28, Opatija, Croatia.
2. Oswal, G.P., & Foong, M. (2006). *RFID vs. contactless smart cards—an unending debate*. Frost & Sullivan, Asia Pacific.
3. Klaus, F. (2003). *RFID handbook* (pp. 22–241). New Jersey: Wiley.
4. Lee, Y. (2003). Ph.D. Microchip Technology Inc. Antenna Circuit Design for RFID Applications [J].
5. Constantine, A.B. (1997). *Antenna theory: Analysis and design* (pp. 203–242). New Jersey: Wiley.

Author Biography

Yejun He (SM'09) received his Ph.D. degree in Information and Communication Engineering from Huazhong University of Science and Technology (HUST) in 2005, M.S. degree in Communication and Information System from Wuhan University of Technology (WHUT) in 2002 respectively, and his B.S. degree from Huazhong University of Science and Technology in 1994. From Sept. 2005 to March 2006, he was a Research Associate with Department of Electronic and Information Engineering, The Hong Kong Polytechnic University. From April 2006 to March 2007, he was a Research Associate with Department of Electronic Engineering, Faculty of Engineering, The Chinese University of Hong Kong. From July 2012 to August 2012, he is a visiting professor with Department of Electrical and Computer Engineering, University of Waterloo, Waterloo, Ontario, Canada. He is currently a Professor of Information and Communication Engineering at Shenzhen University, China. His Research Interests include Channel Coding and Modulation; MIMO-OFDM wireless communication; Space-time processing; Smart antennas and so on. Dr. He is a Senior Member of IEEE, a senior member of China Institute of Communications and China Institute of Electronics as well as a member of Youth Committee of China Institute of Communications. He is also serving/served as reviewer/Technical Program Committee member/Session Chair for various journals and conferences, including IEEE Transactions on Vehicular Technology, IEEE Communications Letters, International Journal of Communication Systems, Wireless Communications and Mobile Computing, Wireless Personal Communication, KSII Transactions on Internet and Information Systems, IEEE VTC (2008-Spring, 2009-Spring and 2012-Fall), IEEE ICCCAS (2007, 2008 and 2009), ICST ChinaCom (2009, 2010 and 2011), APCC (2009 and 2010), ACM IWCMC2010, IEEE WiMob2009, IEEE CSE2010, WCSP2011 and so on. He served as the organizing committee vice chair of the 2010 International Conference on Communications and Mobile Computing (CMC2010) and an editor of the CMC2010 Proceedings. He acted as the publicity chair of IEEE PIMRC 2012. He is the principal investigator in more than 10 current or finished research projects including

NSFC of China, the integration project of production teaching and research by Guangdong Province and Ministry of Education as well as the Science and Technology Program of Shenzhen City and so on. He translated three English books into Chinese and authored or co-authored more than 60 research papers as well as applied for 11 patents since 2002. He has been Associate Editor of Security and Communication Networks since 2012.